


# Revealing divergent length scales using quantum Fisher information in the Kitaev honeycomb model

James Lambert<sup>\*</sup> and Erik S. Sørensen<sup>†</sup>

Department of Physics &amp; Astronomy, McMaster University, 1280 Main St. W., Hamilton, Ontario L8S 4M1, Canada

 (Received 13 September 2020; revised 2 November 2020; accepted 6 November 2020; published 1 December 2020)

We compute the quantum Fisher information (QFI) associated with two different local operators in the ground state of the Kitaev honeycomb model, and find divergent behavior in the second derivatives of these quantities with respect to the driving parameter at the quantum phase transition between the gapped and gapless phases for both fully antiferromagnetic and fully ferromagnetic exchange couplings, thus demonstrating that the second derivative a locally defined, experimentally accessible, QFI can detect topological quantum phase transitions. The QFI associated with a local magnetization operator behaves differently from that associated with a local bond operator depending on whether the critical point is approached from the gapped or gapless side. We show how the behavior of the second derivative of the QFI at the critical point can be understood in terms of the diverging length scales associated to the two and four point correlators of the Majorana degrees of freedom. We present critical exponents associated with the divergences of these length scales.

DOI: [10.1103/PhysRevB.102.224401](https://doi.org/10.1103/PhysRevB.102.224401)

## I. INTRODUCTION

### A. Overview

The quantum Fisher information (QFI)  $\mathcal{F}$  arises naturally in quantum metrology [1–6]. Given a general state  $\rho(\theta)$  where  $\theta$  is some parameter, the QFI bounds the precision with which  $\theta$  may be extracted in *any*  $M$  measurements through the Cramér-Rao bound,  $\text{Var}_\rho(\theta_i) \geq 1/\sqrt{M\mathcal{F}}$ . In other words, the QFI quantifies the extent to which a parameterized state  $\rho(\theta)$  may be distinguished from a neighboring state  $\rho(\theta + d\theta)$ . By quantifying the distinguishability of neighboring states, the QFI furnishes a natural notion of distance on the Hilbert space, with more easily distinguishable states separated by a greater distance. Formally, the QFI quantifies the local change in the Bures distance under the aforementioned parameterization [7–10]. This geometrical interpretation of the QFI expands its scope of application to probing the physics of condensed matter phases and phase transitions [11–17]. The QFI also exhibits interesting behavior during a quantum quench in spin chain systems [18]. In fact, a special case of the QFI is already ubiquitous in theoretical studies of condensed matter systems. The fidelity susceptibility (FS) [19] is directly proportional to the QFI [20] for an appropriate parameterization. In particular, one often considers parameterizations that have been generated unitarily (though this is not the only choice) by a Hermitian operator  $\hat{O}$  according to  $\rho(\theta) = e^{i\theta\hat{O}}\rho e^{-i\theta\hat{O}}$  and we will restrict ourselves to this case here. The operator  $\hat{O}$  is usually expressed as a sum over suboperators  $\hat{O}^\alpha$ ,

$$\hat{O} = \sum_r \hat{O}_r^\alpha. \quad (1)$$

A *local* operator is one for which all  $\hat{O}_r^\alpha$  depend on a contiguous sublattice that is small relative to the total lattice. One may also consider *nonlocal* parameterizations, such as the string operators considered in Ref. [21]. Nonlocal parameterizations reveal remarkable behavior in topological phases as demonstrated in Ref. [21], where a characteristic, superextensive scaling of the nonlocal QFI is demonstrated in the topologically nontrivial phases of the Kitaev wire.

In a many-body state containing  $N$  degrees of freedom, the QFI density  $F = \mathcal{F}/N$  quantifies the degree of multipartite entanglement when the state  $\rho$  is projected into the eigenbasis of the operator  $\hat{O}$  that generates the parameterization. For  $F > m$  where  $m|N$ , we say the state is  $(m + 1)$  partite entangled [4,22,23]. Specifically, for the case of pure states  $\psi$  and unitary parameterizations, the QFI is proportional to the variance of the generator [7]

$$\mathcal{F} = 4\text{Var}_\psi(\hat{O}). \quad (2)$$

While one could perform an interesting study looking only at the variances, we prefer to work within the context of the QFI because it continues to be well defined at finite temperature. This link allows the critical properties of the ground state to be inferred from the thermal scaling of the QFI [12,24]. While we do not consider finite temperature behavior in this study, the connection offers a path forward for future work. Recently, it was shown that the QFI can be detected experimentally in inelastic scattering measurements [12]. Thus working within the context of the a locally defined QFI also allows for connection with experiment. This contributes to a growing body of research on experimental approaches to extract multipartite entanglement [25–27]. We emphasize that we do not detect genuine multipartite entanglement in this study, but mention the connection for completeness.

Given that the QFI is defined at finite temperature and that the zero temperature QFI is proportional to the variance,

\*lambj3@mcmaster.ca

†sorensen@mcmaster.ca

one might ask, what is the generalization of the notion of variance to the finite temperature case? By imagining that the variance of an observable contains a quantum contribution and a thermal contribution, quantum variances (QV) may be defined which are proportional to an upper and lower bounds of the QFI [28]. The QFI at zero temperature can be viewed as the zero-temperature limit of the quantum contribution to the variance (the thermal contribution being zero at zero temperature).

The QFI has now been studied in a wide range of models [12–16]. Of particular interest for our purposes is the work done on the Kitaev wire in Ref. [21], where the first derivative of the QFI associated with a local generator was shown to exhibit a divergence at the topological phase transition of that model, and where the topologically nontrivial phase exhibits superextensive scaling of the QFI associated with a nonlocal generator.

Quantum spin liquids (QSL) are characterized by a lack of any form of long-range magnetic order down to zero temperature [29]. Such phases are thought to exhibit instead subtle forms of quantum ordering, along with topologically nontrivial anyonic excitations [30]. In so far as these phases are characterized by a lack of order, their detection in experiment presents a substantial challenge. In this work we examine the behavior of the QFI in the Kitaev honeycomb model (KHM) [31], which presents two spin liquid phases (one gapped and one gapless), induced by exchange coupling anisotropy.

The KHM has been studied from an information theoretic perspective before, with studies examining the Jensen-Shannon divergence [32] and the mutual information [33]. Of particular interest is the Fidelity susceptibility, which was studied in Ref. [17] and the study of the Bures distance in Ref. [34]. In the case of an  $n$  parameter estimation scenario (or an  $n$ -dimensional unitary parametrization), the Bures distance is locally equivalent to the QFI Matrix which is a Riemannian metric on the Hilbert space [7]. The Fidelity susceptibility is recovered by examining the particular parametrization of the Hilbert space corresponding to the driving operator of the phase transition. The physics of the KHM have also been studied using SU(2) parton approaches [35]. Details of the dynamical response of the model in the presence of magnetic fields may be found in Ref. [36].

For the remainder of this section we introduce the KHM and explain its key features. In Sec. II we discuss the relationship between the scaling of the second derivative of the QFI density (hereafter called the QFI *susceptibility*)  $\partial_u^2 F$ , where  $u$  drives the phase transition and the correlation functions of the generator. In Sec. III we analyze the behavior of these quantities for the *magnetization* operator  $\sum_j S_j^\alpha$  (where  $j$  represents both a unit cell position and sublattice index), in Sec. III A and the *bond*  $\sum_r S_{r,A}^\alpha S_{r,B}^\alpha$ , where  $r$  indicates a unit cell in Sec. III B. Finally, we conclude our discussion in Sec. IV, where we discuss the relevance of this work to studies of the geometric phase.

### B. Kitaev honeycomb model

The Kitaev honeycomb model (KHM) is given by

$$H = \sum_{\langle j,k \rangle} K^{\gamma_{j,k}} S_j^{\gamma_{j,k}} S_k^{\gamma_{j,k}}, \quad (3)$$

where the sum is over nearest-neighbor bonds and  $\gamma \in \{x, y, z\}$  denotes a bond-dependent Ising exchange. If the exchange couplings are sufficiently isotropic ( $|K^\gamma| \leq |K^\alpha| + |K^\beta|$ , for all choices of  $\alpha, \beta, \gamma \in \{x, y, z\}$ ), the spectrum is gapless. In the regime where one exchange coupling is dominant (the opposite inequality), the model is gapped. This phase transition between two topologically different spin liquid phases presents no local order parameter. It is instead associated with a subtle kind of symmetry breaking to do with the structure of the gauge fields themselves [31]. On the gapped side of the transition, the model is mapped onto the lattice gauge Ising model [37], with alternative rows of hexagon plaquettes becoming associated with one of the two excitations in that model (conventionally called  $e$  and  $m$  excitations). In both phases, the spin-spin correlation functions are identically zero beyond nearest neighbor. The model also possesses an extensive number of conserved charges defined by the plaquette operators.

Remarkably, the KHM is analytically solvable [31]. By mapping each spin operator into the space of four Majorana fermions  $\{c, b^x, b^y, b^z\}$  via

$$S_j^\gamma = \frac{i}{4} c_j b_j^\gamma,$$

an extensive number of conserved charges can be constructed, given by  $u_{j,k} = i b_j^{\gamma_{j,k}} b_k^{\gamma_{j,k}}$ . These operators take eigenvalues  $\pm 1$ . Using the above mapping, the KHM becomes

$$H = \frac{i}{4} \sum_{jk} K^{\gamma_{j,k}} u_{jk} c_j c_k. \quad (4)$$

Since the  $u_{j,k}$  commute with the Hamiltonian, we may fix a particular configuration of eigenvalues on each bond, and the problem is reduced to free Majoranas hopping in the gauge fields. The lowest-energy configuration will be the flux free configuration, as follows from Lieb's theorem [38]. We therefore choose to work in the configuration where all  $u_{i,j}$  have eigenvalue  $+1$  (hereafter referred to as the standard gauge). Once we fix a gauge configuration, the model is a simple hopping Hamiltonian, which may be diagonalized by Fourier transforming and then performing a Bogoliubov rotation, where the mixing angle is defined implicitly via

$$\tan(2\theta_q) = \frac{\epsilon_q}{\Delta_q}, \quad (5)$$

where

$$\epsilon_q = K^\alpha \cos(q_x) + K^\beta \cos(q_y) + K^\gamma, \quad (6a)$$

$$\Delta_q = K^\alpha \sin(q_x) + K^\beta \sin(q_y), \quad (6b)$$

where  $\alpha, \beta, \gamma \in \{x, y, z\}$  depending on the choice of which bond acts as the unit cell. Here  $q_x = \mathbf{a} \cdot \mathbf{q}$  and  $q_y = \mathbf{a}_2 \cdot \mathbf{q}$  where  $\mathbf{a}_1$  and  $\mathbf{a}_2$  are any choice of translation vectors on the principle lattice and  $q = \frac{n}{L_x} \mathbf{b}_1 + \frac{m}{L_y} \mathbf{b}_2$ , with  $L_x$  and  $L_y$  the side length of the lattice, is a general vector in the reciprocal space.

We note that the true, physical ground state, must be the symmetrized product over all physically equivalent choices of the gauge fields (i.e., all choice of the gauge fields resulting in zero flux). Following arguments described in Ref. [39], the operators we consider are not dependent on projection into the physical subspace at large system sizes. Details of the solution to the Kitaev model are provided in Appendix B1.

## II. QFI SUSCEPTIBILITY AND DIVERGING LENGTH SCALES

To interpret the divergences at the critical point, consider a generator,  $\hat{O} = \sum_r \hat{O}_r$  where the generators are given by a sum over local products of spins  $\hat{S}_r = \prod_{j \in \Lambda_r} S_{r+\ell_j}^{\alpha_j}$ , where  $\Lambda_r$  is some local, contiguous sublattice. The associated QFI density in a pure state is given by

$$F\{\hat{O}\} = \frac{1}{N} \sum_{r_1, r_2} \langle \mathcal{S}_{r_1} \mathcal{S}_{r_2} \rangle - \langle \mathcal{S}_{r_1} \rangle \langle \mathcal{S}_{r_2} \rangle. \quad (7)$$

Through Kitaev's mapping, we may decompose our spin blocks into a component operating on the flux sector  $\mathcal{B}_r = \prod_{j \in \Lambda_r} b_{r+\ell_j}^{\alpha_j}$  and a component operating on the matter sector  $\mathcal{C}_r = \prod_{j \in \Lambda_r} c_{r+\ell_j}$ ,

$$F\{\hat{O}\} = \frac{1}{N} \sum_{r_1, r_2} \langle \mathcal{B}_{r_1} \mathcal{B}_{r_2} \rangle \langle \mathcal{C}_{r_1} \mathcal{C}_{r_2} \rangle - \langle \mathcal{B}_{r_1} \rangle \langle \mathcal{B}_{r_2} \rangle \langle \mathcal{C}_{r_1} \rangle \langle \mathcal{C}_{r_2} \rangle. \quad (8)$$

Now there are three possible values for the flux sector expectation values. If  $\mathcal{B}_r$  is diagonal in the gauge sector, then the contribution from the gauge sector factorizes and gives an overall prefactor of  $\pm 1$ . If  $\mathcal{B}_r$  is strictly off-diagonal, but  $\mathcal{B}_{r_1} \mathcal{B}_{r_2}$  has diagonal entries, then the situation is the same. Finally, it may be the case that  $\mathcal{B}_{r_1} \mathcal{B}_{r_2}$  has nonzero diagonal elements only for certain separations. Regardless of which scenario is realized, the contribution to the QFI from the flux sector will be independent of  $u$  since the gauge fields commute at all points in the phase diagram. The QFI is then given by a sum over the correlation functions in the matter sector Majorana fermions with some prefactor (which might be  $\pm 1$  or 0 as a function of the separation), determined by the situation above. We adopt the standard ansatz for the matter sector correlations

$$\langle \mathcal{C}_{r_1} \mathcal{C}_{r_2} \rangle = \Xi(r, u) r^{-a} e^{-\frac{r}{\xi(u)}}, \quad (9)$$

where  $a$  is determined by the phase and does not depend explicitly on  $u$ , and  $\xi(u)$  is a length scale associated with correlations between the Majorana operators which depends on the position in the phase diagram.

Taking the assumption that, near the critical point,

$$\xi(u) \sim |u - u_c|^{-\nu} \quad (10)$$

one can show that the second derivative of the QFI density must diverge at the critical point like

$$\partial_u^2 F\{\hat{O}\} \sim |u - u_c|^{\nu-2}. \quad (11)$$

Therefore  $\Delta_{\hat{O}} = \nu - 2$ . The QFI and, by extension, the QFI susceptibility, are, in principle, experimentally accessible probes. In particular for the case of local generator such as the total magnetization operator. The QFI can there be used to extract experimentally the scaling of the correlation length associated with the matter sector of the KHM. This analysis is similar to the analysis performed in the supplementary materials of [12], where the authors examined the effects of coarse-graining transformation on the QFI to arrive a scaling hypothesis for the near field and finite temperature regimes.

In practice, experimentally relevant models will not be amenable to the above treatment, as the KHM acquires additional terms in real materials that break the integrability of

Kitaev's original solution (e.g., Heisenberg terms and symmetric off-diagonal terms) [40]. In these cases the analysis may instead be applied to the correlation length of the spin degrees of freedom directly, and divergences in the QFI susceptibility may still be linked to the critical exponent for the divergence of a correlation length.

## III. QFI SUSCEPTIBILITY FOR MAGNETIZATION AND BOND OPERATORS

Motivated by the results of the authors of Ref. [21], we compute the QFI associated with two local operators and examine the second derivatives of those operators with respect to the driving parameter of the phases transition. In both cases the second derivative of the QFI is found to diverge. We term this the QFI *susceptibility*.

Throughout this section we consider a path through the space of exchange couplings parameterized by  $u$ ,

$$K^z = 1 + u, \quad (12a)$$

$$K^x = 1, \quad (12b)$$

$$K^y = 1. \quad (12c)$$

For this parametrization,  $u_c = 1$  represents the critical point between the gapless phase ( $u < 1$ ) and the gapped phase ( $u > 1$ ). The ground state of the KHM is a function of  $u$  and is hereafter denoted as  $\psi_0(u)$ . We consider the case of fully ferromagnetic and fully antiferromagnetic exchange couplings for both parametrizations (in which case  $K^y \rightarrow -K^y$ ). Unless otherwise noted, calculations are carried out for  $L_x = L_y = 10^4$  with periodic boundary conditions in a rhombic geometry.

### A. Magnetization operator

First we examine the QFI in the Kitaev honeycomb as generated by the magnetization operator

$$\hat{O}_M^\alpha = \sum_r (S_{r,A}^\alpha + S_{r,B}^\alpha), \quad (13)$$

here  $\alpha \in \{x, y, z\}$ ,  $r$  denotes a unit cell in the two site basis, and  $A, B$  denotes the sublattice. The corresponding QFI is given by

$$F_{M,\alpha}(u) \equiv F\{\hat{O}_M^\alpha; \psi_0(u)\} = 4 \text{Var}_{\psi_0}(O_M^\alpha) \quad (14)$$

$$= 1 - \frac{1}{N} \sum_q \cos(2\theta_q) \quad (15)$$

with  $\psi_0(u)$  defined at the start of this section.

Figure 1 shows this quantity plotted along the path defined by Eq. (12c) for the fully antiferromagnetic [Fig. 1(a)] and ferromagnetic [Fig. 1(b)] cases, respectively. In the AFM case the ground state possesses  $F_{M,\alpha} > 1$  for each spin component. This is indicative of at least bipartite entanglement. In a pure state any nonzero QFI is indicative of the presence of quantum correlations. Nonetheless, the QFI in the fully ferromagnetic case is insufficient to witness even bipartite entanglement, indicating that quantum correlations are reduced for the FM coupling.

The absolute values of the derivatives of  $F_{M,\alpha}$  will be the same in the AFM and FM cases. This can be seen by

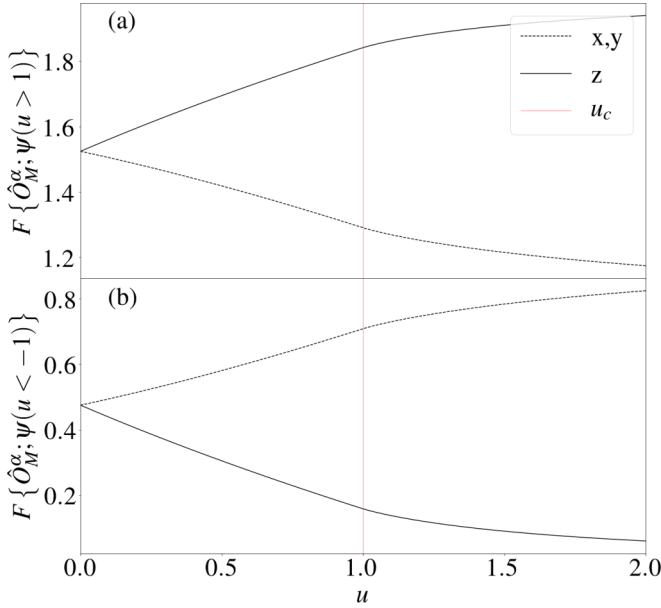


FIG. 1. QFI for Magnetization operator with fully (a) antiferro and (b) ferro magnetic exchange couplings. The red vertical line marks the critical value of  $u$ . Results are for  $L_x = L_y = 10^4$  with a  $u$  spacing of  $\sim 10^{-3}$ .

considering the fact that the functional dependence of  $F_{M,\alpha}$  on the driving parameter  $u$  enters through the nearest-neighbor correlation functions, which are the same in both cases up to a negative sign.

The first and second derivatives of the QFI are given in Fig. 2. We observe that the QFI susceptibility associated with the magnetization operator exhibits a power-law divergence

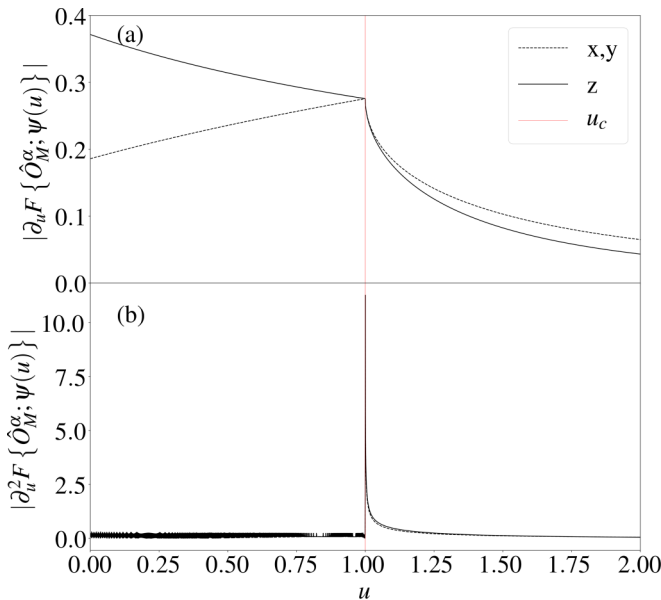


FIG. 2. (a) First and (b) second derivatives of the QFI generated by the magnetization operator. The results are the same in both the ferro and antiferro magnetic cases. Results for  $L_x = L_y = 10^4$  with a  $u$  spacing  $\sim 10^{-3}$ . The red line denotes the position of the critical point.

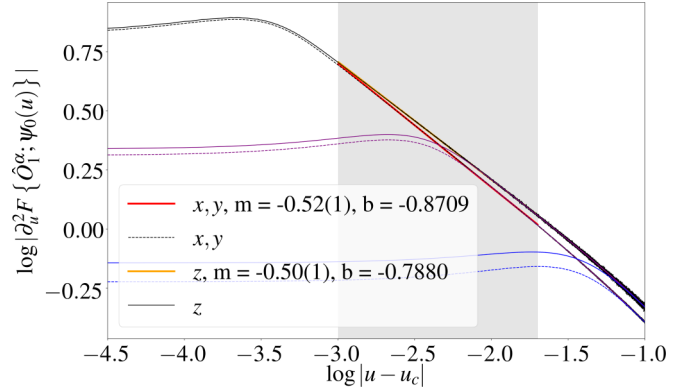


FIG. 3. Log-log plot of the second derivative of the QFI with respect to the magnetization operator and the distance to the critical point from the gapped side ( $u > 1$ ). Results for  $L_x = L_y = 10^4$  with a linear  $\Delta u \sim 10^{-5}$ . The purple and blue curves correspond to system sizes  $L_x = L_y = 10^3$  and  $L_x = L_y = 10^2$ , respectively, and demonstrate that the plateau is a finite-size effect. This regime appears to be valid for approximately the interval  $10^{-1.7} > u > 10^{-3.0}$ .

when approaching the critical point from the gapped side. When approaching the critical point from the gapless side the transition appears first order. The behavior of the transition from the gapped side can be understood in light of the analysis in Sec. II. Using the scaling hypothesis

$$\partial_u^2 F_{M,\alpha}(u) \sim |u - u_c|^{\Delta_{M,\alpha}}, \quad (16)$$

we extract the following critical exponents for the second derivative of the QFI for each spin component of the magnetization operator

$$\Delta_{M,x} = \Delta_{M,y} \approx -0.52(1), \quad (17a)$$

$$\Delta_{M,z} \approx -0.50(1), \quad (17b)$$

and can be seen in Fig. 3 over a region from  $10^{-1.7} > u > 10^{-3.0}$ . At this point finite, finite-size effects enter, and the scaling ansatz is no longer valid. This leads to plateaus in the QFI susceptibility which occur closer to the critical point for larger system sizes as seen from the data in Figs. 3 and 5.

## B. Bond correlation operator

We now turn to the QFI as parameterized by the bond correlation operator

$$\hat{O}_B^\alpha = \sum_r S_{r,A}^\alpha S_{r,B}^\alpha, \quad (18)$$

with the corresponding QFI density given by

$$F_{B,\alpha} = \frac{1}{2N} \sum_q \sin^2(2\theta_q). \quad (19)$$

In this case the AFM and FM cases are identical. We repeat the same analysis as for the magnetization operator as shown in Figs. 4 and 5. The QFI associated with the bond operator along the  $x$  and  $y$  components converges to a constant value immediately following the phase transition, while the QFI associated with the  $z$  component bond operator falls towards zero. This behavior can be understood by the fact that the

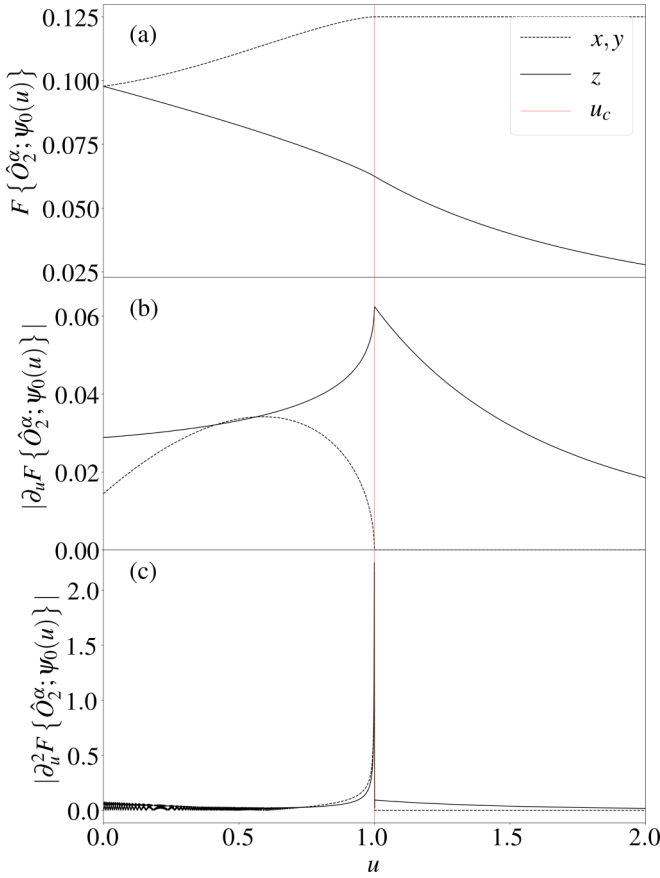


FIG. 4. QFI associated with the (a) bond correlation operator with (b) first and (c) second derivatives. The critical point is marked with a solid vertical red line. The second derivatives diverge, this time approaching the critical point from the left (the gapless phase).

Hamiltonian in the gapped phase is dominated by the Ising exchange on the  $z$  bonds. Consequently, the commutator between the Hamiltonian and the bond operator approaches zero in the limit of  $u \rightarrow \infty$ .

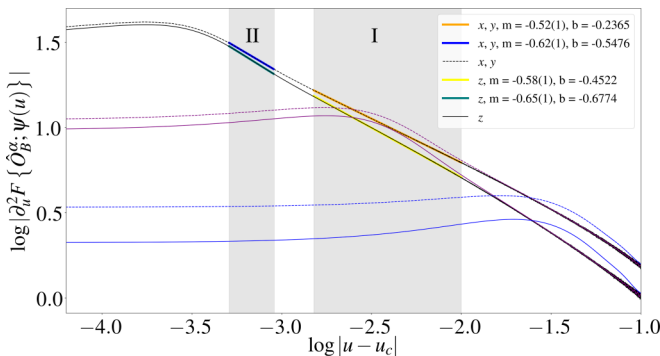


FIG. 5. Log-log plot of the second derivative of the QFI associated with the bond operator versus the distance from the critical point from the gapless phase ( $u < 1$ ). Results are the black curve are for  $L_x = L_y = 10^4$  with a line  $\Delta u \sim 10^{-5}$ . The purple and blue curves correspond to square geometries of size  $L_x = L_y = 10^3$  and  $L_x = L_y = 10^2$ , respectively. The shaded regions (I) and (II) correspond to two regimes where we see linear scaling. The first region is valid for approximately the interval  $10^{-1.9} > u > 10^{-2.8}$ , while the second regime span approximately  $10^{-3.0} > u > 10^{-3.3}$ .

Assuming the same scaling ansatz as for the second derivative  $F_{M,\alpha}$  we find a crossover between two scaling regimes. The first regime is given by the critical exponents

$$\Delta_{B,x}^{(I)} = \Delta_{B,y}^{(I)} \approx -0.52(1), \quad (20a)$$

$$\Delta_{B,z}^{(I)} \approx -0.58(1), \quad (20b)$$

which appears valid on the interval  $10^{-1.9} > u > 10^{-2.8}$  and a second regime characterized by the exponents

$$\Delta_{B,x}^{(II)} = \Delta_{B,y}^{(II)} \approx -0.62(1), \quad (21a)$$

$$\Delta_{B,z}^{(II)} \approx -0.65(1), \quad (21b)$$

which appears to be valid on the interval  $10^{-3.0} > u > 10^{-3.3}$ . While the magnetization operator exhibits a divergence when approaching the critical point from the gapped phase, the bond operator exhibits a divergence approaching the critical point from the gapless phase.

The oscillatory behavior on the gapless side of the transitions for both QFI's is related to divergences in the QFI susceptibility due to points where the denominator of the integrand goes to zero. In the gapped phase these points are necessarily absent.

### C. Diverging length scales

Using the results of the previous section we can determine the scaling of the divergence in the correlation length for  $\langle c_{r_1,A} c_{r_2,B} \rangle$  (using the divergence in the magnetization operator), and for  $\langle c_{r_1,A} c_{r_1,B} c_{r_2,A} c_{r_2,B} \rangle$ .

In light of Eq. (11), we can now understand that the QFI susceptibility associated with the magnetization operator diverges from the gapped side due specifically to the divergence in that correlation function of the matter sector Majorana's. On the gapless side of the transition, the correlation function for the matter sector Majorana's is critical, and consequently the second derivative of Eq. (9) is given specifically by  $\Xi(r, u)$  and contains no divergence.

Using Eq. (11), we may extract the scaling exponents for the correlation length of the matter sector correlation functions in the  $x$  and  $y$ , and  $z$  channels for  $\partial_u^2 F_{M,\alpha}$ ,

$$v_{M,x} = v_{M,y} \approx 1.48(1), \quad (22a)$$

$$v_{M,z} \approx 1.50(1), \quad (22b)$$

and for the two scaling regimes of  $\partial_u^2 F_{B,\alpha}$  for  $u < u_c$ . The first given by

$$v_{B,x}^{(I)} = v_{B,y}^{(I)} \approx 1.48(1), \quad (23a)$$

$$v_{B,z}^{(I)} \approx 1.42(1), \quad (23b)$$

and the second by

$$v_{B,x}^{(II)} = v_{B,y}^{(II)} \approx 1.38(1), \quad (24a)$$

$$v_{B,z}^{(II)} \approx 1.35(1). \quad (24b)$$

## IV. CONCLUSION

We examined the QFI for the bond and magnetization operators in both the gapped and gapless phases of the KHM

and at the transition between these two phases for fully ferromagnetic and fully antiferromagnetic couplings. The second derivative of the QFI with respect to the magnetization operator is shown to diverge when approaching the phase transition from the gapped side like at a second order transition, while the QFI susceptibility approaching the critical point from the gapless side appears first order. Conversely, we find that the QFI susceptibility associated with the bond operator diverges like a second-order transition when approaching the critical point from the gapless side, and like a first-order transition when approaching the critical point from the gapped side.

In both cases, the divergences in the QFI susceptibility can be associated to diverging length scales in the two point correlators of the local generators of the QFI. For the particular case of the KHM, these divergences can be linked to diverging length scales in the matter sector Majorana's, even when the physical spin-spin correlation functions are truncated (as in the case of the two point correlation function). The implication is that the presence of the topological phase transition between the gapped and gapless phases may be detected experimentally at low temperatures.

There has been related work examining the Geometric phase associated with a twist operator acting on both sites [41]. We note that the critical exponents presented in Eq. (21b) for scaling regime (II) of the bond operators are within the margin of error of those in Ref. [41]. Geometrically, the QFI that we compute with respect to the bond operator is the diagonal component of the quantum geometric tensor [42]. The imaginary component of this tensor corresponds to the Berry curvature, while the real component corresponds to the notion of distance induced by the distinguishability of states. In Ref. [43], the connection between these two components of metric was discussed. The implication is that the geometry detected by the Berry phase is intimately related to the geometry of distinguishability, opening the prospect of experimentally measuring the Berry phase in condensed matter systems. Extracting the full quantum metric tensor has recently been achieved in cold atom systems [44].

The QFI associated with the magnetization operator in the fully antiferromagnetic phase is shown to be greater than for the fully ferromagnetic phase, as one would expect from the tendency of the antiferromagnetic coupling to produce spin singlets on the bonds. In the gapped phase defined by large  $K^\gamma$  coupling, the QFI associated with the bond operator converges to a constant value for the QFI generated by the transverse spin components (specifically the  $x$  and  $y$  components in our analysis).

It is shown in Ref. [20] that the QFI is proportional to the FS if the operator parametrizing the QFI is the same as the operator that generates the change in parameter for the ground state. This implies that the QFI for the bond operator from the gapless side of the transition is proportional the FS calculated in Ref. [17], however, we do not find this to be the case. This may be due to the fact that the ground state used in Ref. [17] differs from that used by Kitaev in Ref. [31], which is the one we employ here. Understanding the details of the connection between the QFI and the fidelity susceptibility warrants further investigation. We also note that the definition of the QFI may not be unique when a Hamiltonian possesses a degenerate ground-state manifold. In particular, one can

imagine a situation where the generator of the QFI lifts the degeneracy of this manifold, affecting the results. While in our calculation this ambiguity is not present in the gapped phase, it may affect the results in the gapless phase.

Future research is warranted to examine the behavior of the QFI at finite temperatures around the critical point, where the ground-state scaling will be modified by finite-temperature effects. The connection between the finite-temperature scaling and the length scale of the Majorana fermions in this case may offer insight into the details of candidate Kitaev spin liquid phases in materials where the pure Kitaev Hamiltonian is modified by material relevant terms [40].

## APPENDIX A: SCALING BEHAVIOR OF QFI SUSCEPTIBILITY

Let us work specifically on the case of pure states and unitary QFI. The generator of the QFI is most generally given by

$$\hat{O} = \sum_r \hat{O}_r, \quad (\text{A1})$$

where  $\hat{O}_r$  is an operator associated with the site located at  $r$ . We assume that  $r$  is contiguous and local, that is, it encompasses a finite number of degrees of freedom all lying within a distance  $\ell$  from the site  $r$ . We consider a state  $\psi$  that depends on some parameter  $u$  that drives a phase transition at a value  $u_c = 1$ ,

$$\begin{aligned} f\{\hat{O}, \psi(u)\} &= \frac{1}{N} \sum_{r_1, r_2} \langle \hat{O}_{r_1} \hat{O}_{r_2} \rangle_\psi - \langle \hat{O}_{r_1} \rangle_\psi \langle \hat{O}_{r_2} \rangle_\psi \\ &= \frac{1}{N} \sum_{r_1, r_2} C_{r_1, r_2}(u). \end{aligned} \quad (\text{A2})$$

Let us assume that the model is translation invariant and define  $r := |r_1 - r_2|$ . In general, we may assume that the connected correlation functions can be fit to the following form:

$$C_r(u) = \Xi(r, u) r^{-a} e^{-\frac{r}{\xi(u)}}, \quad (\text{A3})$$

where  $a$  depends on the phase (i.e., is assumed independent of the driving parameter), and  $\xi$  is the correlation length, taken to be a function of the parameter  $u$  (we hereafter drop the explicit dependence). The function  $\Xi(r, u)$  is assumed to be a smooth function of  $r$  and of the parameter  $u$  within a particular phase (though not necessarily smooth at the phase boundary). The divergence in the second derivative of the QFI must emerge from a divergence in the two point correlation functions. We therefore consider the second derivative of Eq. (9)

$$\begin{aligned} \partial_u^2 C_r(u) &= \partial_u (\Xi(r, u) r^{1-a} \xi^{-2} \partial_u \xi e^{-\frac{r}{\xi}} + \partial_u \Xi(r, u) r^{-a} e^{-\frac{r}{\xi}}) \\ &= -2r^{1-a} \Xi(r, u) \xi^{-3} (\partial_u \xi)^2 e^{-\frac{r}{\xi}} \\ &\quad + r^{1-a} \Xi(r, u) \xi^{-2} \partial_u^2 \xi e^{-\frac{r}{\xi}} \\ &\quad + r^{2-a} \Xi(r, u) \xi^{-4} (\partial_u \xi)^2 e^{-\frac{r}{\xi}} + \partial_u^2 \Xi(r, u) r^{-a} e^{-\frac{r}{\xi}} \\ &\quad + \partial_u \Xi(r, u) r^{1-a} \xi^{-2} \partial_u \xi e^{-\frac{r}{\xi}}. \end{aligned} \quad (\text{A4})$$

Naively, the correlation length is expected to diverge at the critical point. Let  $\tilde{u} = |u - u_c|$  be the distance from the critical

point. Then the correlation length goes as

$$\xi \sim \tilde{u}^{-\nu}. \quad (\text{A5})$$

This ansatz may be used to infer the scaling relations for the derivatives of the correlation length

$$\partial_u \xi \sim -\nu \tilde{u}^{-(\nu+1)}, \quad (\text{A6a})$$

$$\partial_u^2 \xi \sim \nu(\nu+1) \tilde{u}^{-(\nu+2)}. \quad (\text{A6b})$$

Substituting this into Eq. (A4) gives

$$\begin{aligned} \partial_u^2 C_r(u) &= -2\Xi(r, u) r^{1-a} \tilde{u}^{3\nu} v^2 \tilde{u}^{-2(\nu+1)} e^{-\frac{r}{\xi}} \\ &\quad + \Xi(r, u) r^{1-a} \tilde{u}^{2\nu} v(\nu+1) \tilde{u}^{-(\nu+1)} e^{-\frac{r}{\xi}} \\ &\quad + \Xi(r, u) r^{2-a} \tilde{u}^{4\nu} v^2 \tilde{u}^{-2(\nu+1)} e^{-\frac{r}{\xi}} \\ &\quad + \partial_u^2 \Xi(r, u) r^{-a} e^{-\frac{r}{\xi}} + \partial_u \Xi(r, u) r^{1-a} \tilde{u}^{2\nu} (-\nu) \\ &\quad \times \tilde{u}^{-(\nu+1)} e^{-\frac{r}{\xi}} \\ &= e^{-\frac{r}{\xi}} (-2\Xi(r, u) r^{1-a} \tilde{u}^{\nu-2} v^2 + \Xi(r, u) r^{1-a} \tilde{u}^{\nu-2} \\ &\quad \times \nu(\nu+1) + \Xi(r, u) r^{2-a} \tilde{u}^{2\nu-2} + \partial_u^2 \Xi(r, u) r^{-a} \\ &\quad - \nu \partial_u \Xi(r, u) r^{1-a} \tilde{u}^{\nu-2}). \end{aligned} \quad (\text{A7})$$

We can now pull out the divergence associated with the proximity to the critical point

$$\begin{aligned} \partial_u^2 C_r(u) &= \tilde{u}^{\nu-2} e^{-\frac{r}{\xi}} (-2\Xi(r, u) r^{1-a} v^2 + \Xi(r, u) r^{1-a} v(\nu+1) \\ &\quad + \Xi(r, u) r^{2-a} \tilde{u}^\nu + \tilde{u}^{2-\nu} \partial_u^2 \Xi(r, u) r^{-a} \\ &\quad - \nu \partial_u \Xi(r, u) r^{1-a}). \end{aligned} \quad (\text{A8})$$

The scaling behavior of the QFI susceptibility is thus given by

$$\partial_u^2 f\{\hat{O}, \psi\} = \tilde{u}^{\nu-2} \zeta(r, u). \quad (\text{A9})$$

We define  $\Delta_\phi = \nu - 2$  as the scaling of the QFI with proximity to the critical point. The y-intercept on the log-log plot will be given by the nonuniversal function  $\zeta(r, u)$ .

## APPENDIX B: CALCULATING VARIANCES

### 1. Solution of the Kitaev model

We adopt the approach of Refs. [39,45], where the Majorana degrees of freedom are recombined into Dirac fermions, with three *bond* fermions

$$b_{r,A}^\gamma = \frac{1}{2} (\beta_r^\gamma + (\beta_r^\gamma)^\dagger), \quad (\text{B1a})$$

$$b_{r,B}^\gamma = \frac{1}{2i} (\beta_r^\gamma - (\beta_r^\gamma)^\dagger), \quad (\text{B1b})$$

and one *matter* fermion

$$c_{r,A} = \frac{1}{2} (f_r + f_r^\dagger), \quad (\text{B2a})$$

$$c_{r,B} = \frac{1}{2} (f_r - f_r^\dagger). \quad (\text{B2b})$$

The bond fermions are not present in the Hamiltonian since we simply replace the bond operators with the eigenvalues of the standard gauge configuration

( $u_{j,k} = 1$ ). The resulting Hamiltonian is quadratic in the matter fermions and translation invariant. It can be diagonalized first by mapping each matter fermion to momentum space,  $f_r = \frac{1}{\sqrt{N}} \sum_q e^{iq \cdot r} f_q$ , and then applying the Bogoliubov rotation,  $f_q = \cos(\theta_q) a_q + i \sin(\theta_q) a_{-q}^\dagger$ , where  $\theta_q$  is defined by

$$\tan(2\theta_q) = \frac{K^x \cos(q_x) + K^y \cos(q_y) + K^z}{K^x \sin(q_x) + K^y \sin(q_y)}. \quad (\text{B3})$$

### 2. Magnetization operator

Begin with

$$\hat{O}_{\text{Mag}}^\alpha = \sum_r \hat{S}_r^\alpha. \quad (\text{B4})$$

The variance is given generally by

$$\langle (\Delta \hat{O})^2 \rangle = \langle O^2 \rangle - \langle O \rangle^2, \quad (\text{B5})$$

which, for the magnetization operator, gives

$$\langle (\Delta \hat{O}_{\text{Mag}}^\alpha)^2 \rangle = \sum_{r_1, r_2} \langle \hat{S}_{r_1}^\alpha \hat{S}_{r_2}^\alpha \rangle. \quad (\text{B6})$$

Using translation invariance and converting the Majorana representation, this expression can be given as

$$\langle (\Delta \hat{O}_{\text{Mag}}^\alpha)^2 \rangle = N \sum_r \langle \hat{S}_0^\alpha \hat{S}_r^\alpha \rangle. \quad (\text{B7})$$

In the Kitaev model, the two-point correlator is zero for all values of  $r$  except nearest neighbors. Thus the sum above can be reduced to

$$\langle (\Delta \hat{O}_{\text{Mag}}^\alpha)^2 \rangle = N \left( \frac{1}{4} + \langle \hat{S}_{0,A}^\alpha \hat{S}_{0,B}^\alpha \rangle \right). \quad (\text{B8})$$

Thus we only need to calculate the nearest-neighbor correlation function

$$\begin{aligned} \langle \hat{S}_{0,A}^\alpha \hat{S}_{0,B}^\alpha \rangle &= \frac{1}{4} \langle \sigma_{0,A}^\alpha \sigma_{0,B}^\alpha \rangle \\ &= \frac{1}{4} \langle (i b_{0,A}^\alpha c_{0,A}) (i b_{0,B}^\alpha c_{0,B}) \rangle \\ &= \frac{1}{4} \langle \mathcal{F} | b_{0,A}^\alpha b_{0,B}^\alpha | \mathcal{F} \rangle \langle \mathcal{M} | c_{0,A} c_{0,B} | \mathcal{M} \rangle \\ &= \frac{1}{4} \langle \mathcal{F} | (-i) (2\hat{n}_0^{\beta\alpha} - 1) | \mathcal{F} \rangle \langle \mathcal{M} | (-i) (2\hat{n}_0^f - 1) | \mathcal{F} \rangle \\ &= -\frac{1}{4} (2\langle \hat{n}_0^f \rangle - 1) \\ &= -\frac{1}{4} \left( 2 \frac{1}{N} \sum_{q_1, q_2} \langle f_{q_1}^\dagger f_{q_2} \rangle - 1 \right) \\ &= -\frac{1}{4} \left( \frac{2}{N} \sum_q \sin^2(\theta_q) - 1 \right). \end{aligned} \quad (\text{B9})$$

The QFI density is four times the variance divided by the system size. Thus

$$f\{\hat{O}_{\text{Mag}}^\alpha\} = 1 + \langle \sigma_{0,A}^\alpha \sigma_{0,B}^\alpha \rangle. \quad (\text{B10})$$

### 3. Bond operator

$$\begin{aligned} \text{Var}(\hat{O}_{2\text{-Site}}^\alpha) &= \langle (\hat{O}_{2\text{-Site}}^\alpha)^2 \rangle - \langle \hat{O}_{2\text{-Site}}^\alpha \rangle^2 \\ &= \sum_{r_1, r_2} \langle \hat{S}_{r_1 A}^\alpha \hat{S}_{r_1 B}^\alpha \hat{S}_{r_2 A}^\alpha \hat{S}_{r_2 B}^\alpha \rangle - \left( \sum_r \hat{S}_{r_1 A}^\alpha \hat{S}_{r_1 B}^\alpha \right)^2 \\ &= \frac{1}{16} \left( \sum_{r_1, r_2} \langle b_{r_1 A}^\alpha b_{r_1 B}^\alpha b_{r_2 A}^\alpha b_{r_2 B}^\alpha \rangle \langle c_{r_1 A} c_{r_1 B} c_{r_2 A} c_{r_2 B} \rangle \right. \\ &\quad \left. - \left( \sum_r -\langle b_{r A}^\alpha b_{r B}^\alpha \rangle \langle c_{r A} c_{r B} \rangle \right)^2 \right). \quad (\text{B11}) \end{aligned}$$

We can compute the flux sector expectation values easily

$$\begin{aligned} \langle b_{r_1 A}^\alpha b_{r_1 B}^\alpha b_{r_2 A}^\alpha b_{r_2 B}^\alpha \rangle &= (-i)^2 \langle (\beta_{r_1} + \beta_{r_1}^\dagger)(\beta_{r_1} - \beta_{r_1}^\dagger)(\beta_{r_2} + \beta_{r_2}^\dagger) \\ &\quad \times (\beta_{r_2} - \beta_{r_2}^\dagger) \rangle \\ &= -\langle (2n_{r_1} - 1)(2n_{r_2} - 1) \rangle \\ &= -1, \quad (\text{B12}) \end{aligned}$$

where the last line follows from the fact that the ground state in the standard flux configuration is defined by  $u_r = 2n_r - 1 = 1$ . Similarly we find

$$\begin{aligned} \langle b_{r A}^\alpha b_{r B}^\alpha \rangle &= (-i) \langle (2n_r - 1) \rangle \\ &= (-i). \quad (\text{B13}) \end{aligned}$$

The variance is therefore

$$\begin{aligned} \text{Var}(\hat{O}_{2\text{-Site}}^\alpha) &= \frac{1}{16} \left( \sum_{r_1, r_2} (-1) \langle c_{r_1 A} c_{r_1 B} c_{r_2 A} c_{r_2 B} \rangle - \left( \sum_r (i) \langle c_{r A} c_{r B} \rangle \right)^2 \right) \\ &= \frac{1}{16} \left( - \sum_{r_1, r_2} \langle c_{r_1 A} c_{r_1 B} c_{r_2 A} c_{r_2 B} \rangle + \sum_{r_1, r_2} \langle c_{r_1 A} c_{r_1 B} \rangle \langle c_{r_2 A} c_{r_2 B} \rangle \right) \\ &= \frac{1}{16} \left( \sum_{r_1, r_2} -\langle c_{r_1 A} c_{r_1 B} \rangle \langle c_{r_2 A} c_{r_2 B} \rangle + \langle c_{r_1 A} c_{r_2 A} \rangle \langle c_{r_1 B} c_{r_2 B} \rangle - \langle c_{r_1 A} c_{r_2 B} \rangle \langle c_{r_1 B} c_{r_2 A} \rangle \langle c_{r_1 A} c_{r_1 B} \rangle \langle c_{r_2 A} c_{r_2 B} \rangle \right) \\ &= \frac{1}{16} \left( \sum_{r_1, r_2} \langle c_{r_1 A} c_{r_2 A} \rangle \langle c_{r_1 B} c_{r_2 B} \rangle - \langle c_{r_1 A} c_{r_2 B} \rangle \langle c_{r_1 B} c_{r_2 A} \rangle \right). \quad (\text{B14}) \end{aligned}$$

We now need only evaluate the two point correlators above. For the first term we have

$$\begin{aligned} \langle c_{r_1 A} c_{r_2 A} \rangle &= \frac{1}{N} \sum_{q_1, q_2} e^{iq_1 r_1} e^{iq_2 r_2} \langle (f_{q_1} + f_{q_1}^\dagger) \rangle \langle (f_{q_2} + f_{q_2}^\dagger) \rangle \\ &= \frac{1}{N} \sum_{q_1, q_2} e^{iq_1 r_1} e^{iq_2 r_2} \langle f_{q_1} f_{q_2} + f_{q_1} f_{q_2}^\dagger + f_{q_1}^\dagger f_{q_2} \\ &\quad + f_{q_1}^\dagger f_{q_2}^\dagger \rangle \\ &= \frac{1}{N} \sum_{q_1, q_2} e^{iq_1 r_1} e^{iq_2 r_2} \langle f_{q_1} f_{q_2} + f_{q_1}^\dagger f_{q_2}^\dagger + \delta_{q_1, q_2} \rangle. \quad (\text{B15}) \end{aligned}$$

We can see that

$$\begin{aligned} \langle f_{q_1} f_{q_2} \rangle &= i \cos(\theta_{q_1}) \sin(\theta_{q_2}) \langle a_{q_1} a_{-q_2}^\dagger \rangle \\ &= i \cos(\theta_{q_1}) \sin(\theta_{q_2}) \delta_{q_1, -q_2}, \end{aligned}$$

$$\begin{aligned} \langle f_{q_1}^\dagger f_{q_2}^\dagger \rangle &= (-i) \cos(\theta_{q_1}) \sin(\theta_{q_2}) \langle a_{-q_1} a_{q_2}^\dagger \rangle \\ &= (-i) \cos(\theta_{q_1}) \sin(\theta_{q_2}) \delta_{-q_1, q_2}. \quad (\text{B16}) \end{aligned}$$

Consequently,

$$\begin{aligned} \langle c_{r_1 A} c_{r_2 A} \rangle &= \frac{1}{N} \sum_{q_1, q_2} e^{iq_1 r_1} e^{iq_2 r_2} \delta_{q_1, q_2} \\ &= \frac{1}{N} \sum_q e^{iq(r_1 - r_2)} = \delta_{r_1, r_2}. \quad (\text{B17}) \end{aligned}$$

Similarly we may show that

$$\langle c_{r_1 B} c_{r_2 B} \rangle = \delta_{r_1, r_2}. \quad (\text{B18})$$



For the second term we begin with

$$\begin{aligned}
\langle c_{r_1 A} c_{r_2 B} \rangle &= \frac{1}{N} \sum_{q_1, q_2} e^{iq_1 r_1} e^{iq_2 r_2} (-i) (f_{q_1} + f_{q_1}^\dagger) (f_{q_2} - f_{q_2}^\dagger) \\
&= \frac{1}{N} \sum_{q_1, q_2} e^{iq_1 r_1} e^{iq_2 r_2} (-i) (f_{q_1} f_{q_2} - f_{q_1} f_{q_2}^\dagger + f_{q_1}^\dagger f_{q_2} - f_{q_1}^\dagger f_{q_2}^\dagger) \\
&= \frac{(-i)}{N} \sum_{q_1, q_2} e^{iq_1 r_1} e^{iq_2 r_2} ((f_{q_1} f_{q_2} - f_{q_1}^\dagger f_{q_2}^\dagger) + (f_{q_1}^\dagger f_{q_2} - f_{q_1} f_{q_2}^\dagger)) \\
&= \frac{(-i)}{N} \sum_{q_1, q_2} e^{iq_1 r_1} e^{iq_2 r_2} ((f_{q_1} f_{q_2} - f_{q_1}^\dagger f_{q_2}^\dagger) + (2f_{q_1}^\dagger f_{q_2} - 1)) \\
&= \frac{(-i)}{N} \sum_{q_1, q_2} e^{iq_1 r_1} e^{iq_2 r_2} [i \cos(\theta_{q_1}) \sin(\theta_{q_2}) (\delta_{q_1, -q_2} + \delta_{-q_1, q_2}) + 2 \sin(\theta_{q_1}) \sin(\theta_{q_2}) \delta_{q_1, q_2} - 1] \\
&= \frac{(-i)}{N} \sum_q 2i e^{-iq(r_1 - r_2)} \cos(\theta_q) \sin(\theta_q) + \frac{(-i)}{N} \sum_q [2 \sin^2(\theta_q) - 1] \\
&= \frac{1}{N} \sum_q e^{-iq(r_1 - r_2)} 2 \cos(\theta_q) \sin(\theta_q) + \frac{i}{N} \sum_q e^{iq(r_1 + r_2)} \cos(2\theta_q) \\
&= \frac{1}{N} \sum_q e^{-iq(r_1 - r_2)} \sin(2\theta_q) + \frac{i}{N} \sum_q e^{iq(r_1 + r_2)} \cos(2\theta_q). \tag{B19}
\end{aligned}$$

The final two-point correlator is given by

$$\begin{aligned}
\langle c_{r_1 B} c_{r_2 A} \rangle &= \frac{1}{N} \sum_{q_1, q_2} e^{iq_1 r_1} e^{iq_2 r_2} (-i) (f_{q_1} - f_{q_1}^\dagger) (f_{q_2} + f_{q_2}^\dagger) \\
&= \frac{(-i)}{N} \sum_{q_1, q_2} e^{iq_1 r_1} e^{iq_2 r_2} ((f_{q_1} f_{q_2} - f_{q_1}^\dagger f_{q_2}^\dagger) - (2f_{q_1}^\dagger f_{q_2} - 1)) \\
&= \frac{(-i)}{N} \sum_{q_1, q_2} e^{iq_1 r_1} e^{iq_2 r_2} [i \cos(\theta_{q_1}) \sin(\theta_{q_2}) (\delta_{q_1, -q_2} + \delta_{-q_1, q_2}) - [2 \sin(\theta_{q_1}) \sin(\theta_{q_2}) \delta_{q_1, q_2} - 1]] \\
&= \frac{(-i)}{N} \sum_q 2i e^{-iq(r_1 - r_2)} \cos(\theta_q) \sin(\theta_q) - \frac{(-i)}{N} \sum_q e^{iq(r_1 + r_2)} [2 \sin^2(\theta_q) - 1] \\
&= \frac{1}{N} \sum_q e^{-iq(r_1 - r_2)} \sin(2\theta_q) - \frac{i}{N} \sum_q e^{iq(r_1 + r_2)} \cos(2\theta_q). \tag{B20}
\end{aligned}$$

The final term is therefore a product of differences

$$\begin{aligned}
\langle c_{r_1 B} c_{r_2 A} \rangle \langle c_{r_1 A} c_{r_2 B} \rangle &= \frac{1}{N^2} \sum_{q_1, q_2} [e^{-i(q_1 + q_2)(r_1 - r_2)} \sin(2\theta_{q_1}) \sin(2\theta_{q_2}) + e^{i(q_1 + q_2)(r_1 + r_2)} \cos(2\theta_{q_1}) \cos(2\theta_{q_2})] \\
&= \frac{1}{N^2} \sum_{q_1, q_2} [e^{ir_1(q_1 + q_2)} e^{-ir_2(q_1 + q_2)} \sin(2\theta_{q_1}) \sin(2\theta_{q_2}) + e^{ir_1(q_1 + q_2)} e^{ir_2(q_1 + q_2)} \cos(2\theta_{q_1}) \cos(2\theta_{q_2})]. \tag{B21}
\end{aligned}$$

Under the summation, we may extract the delta functions

$$\begin{aligned}
\sum_{r_1, r_2} \langle c_{r_1 B} c_{r_2 A} \rangle \langle c_{r_1 A} c_{r_2 B} \rangle &= \frac{1}{N} \sum_{r_2} \sum_{q_1, q_2} \delta_{q_1, -q_2} e^{-ir_2(q_1 + q_2)} \sin(2\theta_{q_1}) \sin(2\theta_{q_2}) + \delta_{q_1, -q_2} e^{ir_2(q_1 + q_2)} \cos(2\theta_{q_1}) \cos(2\theta_{q_2}) \\
&= \sum_q \cos^2(2\theta_q) - \sin^2(2\theta_q). \tag{B22}
\end{aligned}$$

We are now ready to return to our original expression for the variance which reads

$$\begin{aligned}\text{Var}(\hat{O}_{2\text{-Site}}^\alpha) &= \frac{1}{16} \left( N - \sum_q [\cos^2(2\theta_q) - \sin^2(2\theta_q)] \right) \\ &= \frac{1}{16} \sum_q [1 - \cos^2(2\theta_q) + \sin^2(2\theta_q)] \\ &= \frac{1}{8} \sum_q \sin^2(2\theta_q).\end{aligned}\quad (\text{B23})$$

Thus the associated QFI density is

$$\mathcal{F}(\hat{O}_{2\text{-Site}}^\alpha) = 4 \frac{\text{Var}(\hat{O}_{2\text{-Site}}^\alpha)}{N} = \frac{1}{2} \frac{1}{N} \sum_q \sin^2(\theta_q), \quad (\text{B24})$$

passing to the continuum limit we find

$$\mathcal{F}(\hat{O}_{2\text{-Site}}^\alpha) = \frac{1}{2} \int_{\text{BZ}} \sin^2(2\theta_q) d^2 q. \quad (\text{B25})$$

### APPENDIX C: DERIVATIVES OF THE QFI SUSCEPTIBILITY MOMENTUM DENSITY

To gain more insight into the divergence in  $F_{M,\alpha}$ , we define the QFI *momentum density* for the magnetization operator,  $f_{M,\alpha}$  via

$$F_{M,\alpha} = \sum_q \left( \frac{1}{N} - \cos(2\theta_q) \right) = \sum_q f_{M,\alpha}(q; u). \quad (\text{C1})$$

We may explicitly evaluate the first and second derivatives of this quantity for each spin component, giving

$$\partial_u f_{M,x} = \frac{\Delta_x^2 \cos(q_y) - \varepsilon_x \Delta_x \sin(q_y)}{(\varepsilon_x^2 + \Delta_x^2)^{\frac{3}{2}}}, \quad (\text{C2a})$$

$$\partial_u f_{M,y} = \frac{\Delta_y^2 \cos(q_x) - \varepsilon_y \Delta_y \sin(q_x)}{(\varepsilon_y^2 + \Delta_y^2)^{\frac{3}{2}}}, \quad (\text{C2b})$$

$$\partial_u f_{M,z} = \frac{\Delta_z^2}{(\varepsilon_z^2 + \Delta_z^2)^{\frac{3}{2}}}, \quad (\text{C2c})$$

for the first derivatives, and

$$\partial_u^2 f_{M,x} = \frac{-3\varepsilon_x \Delta_x^2 \cos^2(q_y) + \Delta_x [3(\varepsilon_x^2 - \Delta_x^2) + \varepsilon_x + \Delta_x] \sin(q_y) \cos(q_y) + \varepsilon_x (2\Delta_x^2 - \varepsilon_x^2) \sin^2(q_y)}{(\varepsilon_x^2 + \Delta_x^2)^{\frac{5}{2}}}, \quad (\text{C3a})$$

$$\partial_u^2 f_{M,y} = \frac{-3\varepsilon_y \Delta_y^2 \cos^2(q_x) + \Delta_y [3(\varepsilon_y^2 - \Delta_y^2) + \varepsilon_y + \Delta_y] \sin(q_x) \cos(q_x) + \varepsilon_y (2\Delta_y^2 - \varepsilon_y^2) \sin^2(q_x)}{(\varepsilon_y^2 + \Delta_y^2)^{\frac{5}{2}}}, \quad (\text{C3b})$$

$$\partial_u^2 f_{M,z} = \frac{-3\varepsilon_z \Delta_z^2}{(\varepsilon_z^2 + \Delta_z^2)^{\frac{5}{2}}}, \quad (\text{C3c})$$

for the second derivatives. We again compute explicitly the first and second derivatives of the QFI with respect to the driving parameter by rewriting the QFI in terms of an integral over a QFI density

$$F_{B,\alpha} = \int_{\text{BZ}} f_{B,\alpha}(q; u)$$

finding

$$\partial_u f_{B,x} = \frac{\Delta_x \varepsilon_x [\varepsilon_x \sin(q_y) - \Delta_x \cos(q_y)]}{(\varepsilon_x^2 + \Delta_x^2)^2}, \quad (\text{C4a})$$

$$\partial_u f_{B,y} = \frac{\Delta_y \varepsilon_y [\varepsilon_y \sin(q_x) - \Delta_y \cos(q_x)]}{(\varepsilon_y^2 + \Delta_y^2)^2}, \quad (\text{C4b})$$

$$\partial_u f_{B,z} = \frac{\Delta_z^2 \varepsilon_z}{(\varepsilon_z^2 + \Delta_z^2)^2}, \quad (\text{C4c})$$

for the first derivatives and

$$\partial_u^2 f_{B,x} = \frac{[\varepsilon_x \sin(q_y) - \Delta_x \cos(q_y)] \left( [\Delta_x^2 - 3\varepsilon_x^2] \Delta_x \cos(q_y) + (\varepsilon_x^2 - 3\Delta_x^2) \varepsilon_x \sin(q_y) \right)}{(\varepsilon_x^2 + \Delta_x^2)^3}, \quad (\text{C5a})$$

$$\partial_u^2 f_{B,y} = \frac{[\varepsilon_y \sin(q_x) - \Delta_y \cos(q_x)] \left( [\Delta_y^2 - 3\varepsilon_y^2] \Delta_y \cos(q_x) + (\varepsilon_y^2 - 3\Delta_y^2) \varepsilon_y \sin(q_x) \right)}{(\varepsilon_y^2 + \Delta_y^2)^3}, \quad (\text{C5b})$$

$$\partial_u^2 f_{B,z} = \frac{\Delta_z^2 (\Delta_z^2 - 3\varepsilon_z^2)}{(\varepsilon_z^2 + \Delta_z^2)^3}. \quad (\text{C5c})$$

- [1] D. Petz and C. Sudár, *J. Math. Phys.* **37**, 2662 (1996).
- [2] D. Petz, *J. Phys. A: Math. Gen.* **35**, 929 (2002).
- [3] M. G. A. Paris, *Int. J. Quantum. Inform.* **07**, 125 (2009).
- [4] G. Tóth, *Phys. Rev. A* **85**, 022322 (2012).
- [5] G. Tóth and D. Petz, *Phys. Rev. A* **87**, 032324 (2013).
- [6] G. Tóth and I. Apellaniz, *J. Phys. A: Math. Theor.* **47**, 424006 (2014).
- [7] A. S. Holevo, *Statistical Structure of Quantum Theory* (Springer Science & Business Media, New York, 2003), Vol. 67.
- [8] I. Bengtsson and K. Życzkowski, *Geometry of Quantum States: An Introduction to Quantum Entanglement* (Cambridge University Press, Cambridge, England, 2017).
- [9] W. K. Wootters, *Phys. Rev. D* **23**, 357 (1981).
- [10] S. L. Braunstein and C. M. Caves, *Phys. Rev. Lett.* **72**, 3439 (1994).
- [11] P. Zanardi, P. Giorda, and M. Cozzini, *Phys. Rev. Lett.* **99**, 100603 (2007).
- [12] P. Hauke, L. Tagliacozzo, and P. Zoller, *Nat. Phys.* **12**, 778 (2016).
- [13] W.-F. Liu, J. Ma, and X. Wang, *J. Phys. A: Math. Theor.* **46**, 045302 (2013).
- [14] Q. Zheng, Y. Yao, and X.-W. Xu, *Commun. Theor. Phys.* **63**, 279 (2015).
- [15] J. Ma and X. Wang, *Phys. Rev. A* **80**, 012318 (2009).
- [16] J. Lambert and E. S. Sørensen, *Phys. Rev. B* **99**, 045117 (2019).
- [17] S. Yang, S.-J. Gu, C.-P. Sun, and H.-Q. Lin, *Phys. Rev. A* **78**, 012304 (2008).
- [18] R. Jafari and A. Akbari, *Phys. Rev. A* **101**, 062105 (2020).
- [19] P. Zanardi and N. Paunković, *Phys. Rev. E* **74**, 031123 (2006).
- [20] J. Liu, H.-N. Xiong, F. Song, and X. Wang, *Physica A* **410**, 167 (2014).
- [21] L. Pezze, M. Gabbriellini, L. Lepori, and A. Smerzi, *Phys. Rev. Lett.* **119**, 250401 (2017).
- [22] P. Hyllus, W. Laskowski, R. Krischek, C. Schwemmer, W. Wieczorek, H. Weinfurter, L. Pezzé, and A. Smerzi, *Phys. Rev. A* **85**, 022321 (2012).
- [23] L. Pezzé and A. Smerzi, *Phys. Rev. Lett.* **102**, 100401 (2009).
- [24] M. Gabbriellini, A. Smerzi, and L. Pezzè, *Sci. Rep.* **8**, 15663 (2018).
- [25] M. Cramer, M. B. Plenio, and H. Wunderlich, *Phys. Rev. Lett.* **106**, 020401 (2011).
- [26] P. Krammer, H. Kampermann, D. Bruß, R. A. Bertlmann, L. C. Kwek, and C. Macchiavello, *Phys. Rev. Lett.* **103**, 100502 (2009).
- [27] O. Marty, M. Epping, H. Kampermann, D. Bruß, M. B. Plenio, and M. Cramer, *Phys. Rev. B* **89**, 125117 (2014).
- [28] I. Frérot and T. Roscilde, *Phys. Rev. B* **94**, 075121 (2016).
- [29] L. Savary and L. Balents, *Rep. Prog. Phys.* **80**, 016502 (2016).
- [30] X.-G. Wen, *Phys. Rev. B* **65**, 165113 (2002).
- [31] A. Kitaev, *Ann. Phys. (NY)* **321**, 2 (2006), January Special Issue.
- [32] Q. Chen, G.-Q. Zhang, J.-Q. Cheng, and J.-B. Xu, *Quant. Info. Proc.* **18**, 8 (2019).
- [33] J. Cui, J.-P. Cao, and H. Fan, *Phys. Rev. A* **82**, 022319 (2010).
- [34] D. F. Abasto and P. Zanardi, *Phys. Rev. A* **79**, 012321 (2009).
- [35] F. J. Burnell and C. Nayak, *Phys. Rev. B* **84**, 125125 (2011).
- [36] D. A. S. Kaib, S. M. Winter, and R. Valentí, *Phys. Rev. B* **100**, 144445 (2019).
- [37] M. Kardar, *Statistical Physics of Fields* (Cambridge University Press, Cambridge, England, 2007).
- [38] E. H. Lieb, in *Condensed Matter Physics and Exactly Soluble Models* (Springer, New York, 2004), pp. 79–82.
- [39] G. Baskaran, S. Mandal, and R. Shankar, *Phys. Rev. Lett.* **98**, 247201 (2007).
- [40] J. G. Rau, E. K.-H. Lee, and H.-Y. Kee, *Phys. Rev. Lett.* **112**, 077204 (2014).
- [41] J. Lian, J.-Q. Liang, and G. Chen, *Eur. Phys. J. B* **85**, 207 (2012).
- [42] J. Provost and G. Vallee, *Commun. Math. Phys.* **76**, 289 (1980).
- [43] G. Palumbo and N. Goldman, *Phys. Rev. Lett.* **121**, 170401 (2018).
- [44] X. Tan, D.-W. Zhang, Z. Yang, J. Chu, Y.-Q. Zhu, D. Li, X. Yang, S. Song, Z. Han, Z. Li, Y. Dong, H.-F. Yu, H. Yan, S.-L. Zhu, and Y. Yu, *Phys. Rev. Lett.* **122**, 210401 (2019).
- [45] J. Knolle, D. L. Kovrizhin, J. T. Chalker, and R. Moessner, *Phys. Rev. B* **92**, 115127 (2015).